2016-08-08

Application of Voltammetry for Electroanalytical Measurement of Concentrations in LaCl3-MgCl2 Mixtures in Eutectic LiCl-KCl

Zhonghang Wang
University of Chinese Academy of Sciences

Devin Rappleye
University of Utah, drapp@byu.edu

C S. Yang
Jiangxi University of Science and Technology

Michael Simpson
University of Utah, michael.simpson@utah.edu

Original Publication Citation

Wang, Z., Rappleye, D., Yang, C. S., & Simpson, M. F. (2016). Application of Voltammetry for Electroanalytical Measurement of Concentrations in LaCl3-MgCl2 Mixtures in Eutectic LiCl-KCl. Journal of The Electrochemical Society, 163(10), H921. https://doi.org/10.1149/2.0351610jes

Application of Voltammetry for Electroanalytical Measurement of Concentrations in $LaCl_3$-$MgCl_2$ Mixtures in Eutectic LiCl-KCl

Z. Wang[a,b,c], D. Rappleye[a], C. S. Yang[a,d], and M.F. Simpson[a]

[a] Department of Metallurgical Engineering, University of Utah, Salt Lake City, UT 84112, USA

[b] National Engineering Laboratory for Hydrometallurgical Cleaner Production Technology, Institute of Process Engineering, Chinese Academy of Sciences, Beijing 100190, China

[c] University of Chinese Academy of Sciences, Beijing 100049, China

[d] School of Metallurgy and Chemical Engineering, Jiangxi University of Science and Technology, Ganzhou 341000, Jiangxi, China

Abstract

For electroanalytical measurement of molten chloride salts, various voltammetry methods have been used on mixtures of $MgCl_2$ and $LaCl_3$ in eutectic LiCl-KCl. These salt mixtures are of primary interest to spent nuclear fuel electrorefining systems. $MgCl_2$ is used as a surrogate for $PuCl_3$, while $LaCl_3$ represents rare earth fission product salts. Cyclic voltammetry scans with these salt mixtures exhibited extra peaks, presumably due to underpotential deposition of La(III) ions onto Mg. Quantitatively, the current contribution from each peak was best determined using normal pulse voltammetry and fit to the Cottrell equation. This yielded linear correlations for concentration versus diffusional current with very high correlation factors. Applying this method, it was determined that concentration measurement error was less than 4% for both $MgCl_2$ and $LaCl_3$.

Key words: molten salt; voltammetry; concentration prediction; nuclear fuel reprocessing; electrorefining

Introduction

Metal chloride salts dissolved in eutectic LiCl-KCl play a key role in the pyrometallurgical treatment of spent nuclear fuel, commonly known as pyroprocessing. The central unit in the pyroprocessing flowsheet is the electrorefiner (ER), where metallic spent fuel is anodically dissolved with simultaneous cathodic deposition of uranium or uranium mixed with transuranic actinides. [1] At the onset of operation, the electrolyte consists of 5-10 wt% UCl_3 in eutectic LiCl-KCl. With each batch of spent fuel processed, the UCl_3 oxidizes active metal fission products to form alkaline, alkali earth, rare earth, and actinide chlorides in the molten salt. This progressive contaminating of the salt gradually changes its physiochemical properties such as density, liquidus temperature, viscosity, etc. The operator needs feedback from the ER system to determine when to withdraw contaminated salt and replace it with clean LiCl-KCl or LiCl-KCl-UCl_3. Idaho National Laboratory has been processing spent fuel from Experimental Breeder Reactor-II since 1996 using two electrorefiner systems installed in their Fuel Conditioning Facility. [2] INL tracks the composition of the salt in these two ER systems via a combination of sampling/destructive analysis and running a mass tracking computer model. [3] It has been widely recognized that this approach would be unsuitable for a commercial pyroprocessing facility with regards to process control as well as nuclear material safeguards. A pyroprocessing facility in a non-nuclear weapons state would be subject to safeguarding by the International Atomic Energy Agency (IAEA), which has challenging significant quantity and timeliness criteria for assuring safeguards compliance. The INL approach largely relies upon the mass tracking system to predict changes to the ER salt composition in between sample analysis-based verification, which can take months to complete.

For real time analysis of the molten salt in an electrorefiner, voltammetry has been widely investigated. Reports in the literature date back to 2001 when Iizuka et al.[4] published

results of their study of application of square wave and normal pulse voltammetry to mixtures of actinide chlorides in molten LiCl-KCl. It was observed that SWV response was only linear at low concentrations (below the normal level for electrorefining), but differentiated NPV response maintained linearity over a wider range of concentrations (up to 3 wt%). However, this range still does not reach the level which would be used in normal electrorefiner operations. A positive finding was that the measured values of actinide concentrations were not affected by the presence of rare earth chlorides in the salt, which have similar electrochemical reduction potential in molten chloride salt mixtures.

Tylka et. al. published their research results in 2015 for application of cyclic voltammetry (CV) to UCl_3 and $PuCl_3$ concentration measurement in molten LiCl-KCl.[5] They demonstrated that careful adherence to strict electrochemical measurement and data analysis procedure allowed for the CV method to be utilized for accurate concentration measurement. This included properly cleaning electrodes, precisely measuring differential electrode surface area, and applying semi-differentiation to the CV signals to better de-convolute peaks. However, they noted that the diffusion coefficients of the actinides decrease with increasing concentration, which requires independent measurement of the diffusion coefficient and significantly complicates the analysis to determine concentration from a single measurement.

Kim et. al. employed CV and chronoamperometry (CA) to develop a real-time monitoring system for molten salt in electrorefiners.[6] While they successfully extended the concentration correlations up to 9 wt% via empirical correlations, they examined only a single solute ($NdCl_3$) in the molten salt mixture. They found repeating chronoamperometry (RCA) to be particular effective for developing linear correlations up

to high concentrations. However, it has limited application to systems with only a single reduction reaction.

Our group has recently been studying the application of voltammetry to electrorefiner salt mixtures in which two metal cations will reduce within the range of potentials scanned.[7,8] The objective is to evaluate the suitability of voltammetry to complex salt mixtures and optimize the method parameters based on simultaneous measurement of the concentration of two metals in the salt. This is the first step towards moving on to many-component systems comprised of lanthanides and actinides. Difference in standard reduction potential for any two active metal cations is expected to be an important characteristic of these systems, so we examined both close spacings (La-Gd) and wide spacings (La-Th). In the case of close reduction potential pairs, severe CV peak overlap was observed.[7] Semi-differentiation followed by peak fitting was used to determine the individual CV peak heights.[7] Principle component regression was also applied to correlate convoluted CV peaks to concentration. For this system, the concentration predictions exhibited relatively high error. For systems with larger spacing between the reduction potentials, peak separation is much simpler. But two problems can be observed with high reduction potential spacings—under potential deposition (UPD) peaks and working electrode area growth. We accommodated the UPD by running NPV and determining diffusionalcurrent for each reaction, including UPD.[8] NPV is also in theory useful for mitigating area growth, since it involves periodic stripping cycles. While the method described by Tylka et. al. was used for electrode area determination, direct use of diffusion-limited electrode kinetics equations such as the Berzins-Delahay or the Cottrell equation is limited by the variability of diffusion coefficients.[5] If such variability is only a function of the ion of interest, then it should be possible to accommodate for it in empirical concentration correlations that do not require prior knowledge of diffusion coefficients. In the case of La-Th, those correlations proved to be moderately accurate with relative error ranging

from about 1-8%. It is that approach that we continue to investigate in this paper, but now applying to the intermediate reduction potential spacing case of Mg/La in LiCl-KCl.

Experimental

Chemicals/Materials

Salt mixtures were prepared by weighing out known masses of anhydrous lithium chloride/potassium chloride eutectic beads (SAFC-Hitech, 99.99%), anhydrous lanthanum chloride (Alfa Aesar, 99.99% (REO)), and anhydrous magnesium chloride (Alfa Aesar, 99.99%). For preparation of reference electrodes, silver chloride (Strem Chemicals, 99.9%) was obtained in a brown glass bottle and was stored in a dark paper box to protect it from light-induced degradation. After receipt, all chemicals were stored and handled in a dry atmosphere argon glovebox (Innovative Technologies, PureLab HE 4) typically maintained with H_2O and O_2 concentrations of less than 1 ppm.

The melt of LiCl-KCl-$LaCl_3$-$MgCl_2$ was prepared by directly adding a predetermined amount of $LaCl_3$ and $MgCl_2$ powder into the LiCl-KCl eutectic beads followed by heating the mixture to 500^{o}C in an auto electro-melt furnace (Kerr).

A polished tungsten rod (OD=2 mm, 99.95%, Alfa Aesar) was used as the working electrode, and a cylindrical stainless steel basket (D=7 mm, L=10 mm, homemade) containing a polished magnesium rod (OD=6.35 mm, L=25.4 mm, 99.95%, Alfa Aesar) was used as the counter electrode. The reference electrode (RE) was fabricated by inserting a silver wire (D=1 mm, 99.99%, Alfa Aesar) into a mixture of LiCl-KCl-AgCl (5 mol.%), contained in a Mullite tube (D=6.35mm, L=18 mm, CoorsTek). The upper end of the tube was sealed by a tapered cylindrical silicone stopper, through which the Ag wire was held vertically suspended.

Experimental apparatus and procedures

All the experimental tests were carried out by heating the alumina crucible (AdValue Technology, Part No. AL-2100) containing the salt mixtures in the Kerr furnace. This furnace was operated in the aforementioned argon atmosphere glovebox. Electrodes were inserted into the salt from above through an opening in the top of the furnace using electrode guides with fixed spacing.

After the temperature of the eutectic mixture stabilized at 500^{o}C, as measured directly in the salt with an internal thermocouple (Omega, Part No. KQXL-116G-12), the electrodes (WE, RE and CE) were connected to electrical feedthroughs on the glove box which were connected to an Autolab potentiostat (PGSTAT302N) that was controlled by Nova software (Version 1.11) run on a Windows PC laptop. Cyclic voltammetry (CV) and chronoamperometry (CA) cleaning were applied sequentially and repeatedly, till the responding signals were smooth and without any singularity. After the determination of the immersion depth of WE by using a VXM stepping motor controller (Velmex), a series of voltammetry experiments were performed, of which CV scans were recorded for potential range from -1.1 to -2.38 V (or -2.35 V) with various scan rates. CP scans were recorded by applying various cell currents to the system. Immediately following the CP, the cell current was set to zero, and the OCP was recorded. In the CA test, potentials ranging from -1.90 to -2.40 V with a step of -0.10 V were applied to the system. In the normal pulse voltammetry test, the same potential range was applied with a step of 0.01 V, and various pulse times were applied with a fixed interval time of 10 s.

After all the voltammetry experiments were performed. Samples of the salt were taken to verify the composition via analysis using an inductively coupled plasma optimal emission spectroscopy (ICP-OES) instrument (Spectro Genesis, Model No. 20.05.2009).

Results and discussion

Cyclic Voltammetry

Figure 1 shows a CV scan recorded on a tungsten electrode in the LiCl-KCl-$LaCl_3$ ($5.80x10^{-5}$ mol/cm^3)-$MgCl_2$ ($5.61x10^{-5}$ mol/cm^3) melt overlaid onto the one obtained in the pure LiCl-KCl melt at 773 K.

In the pure LiCl-KCl melt, only the solvent decomposition reactions are observed at -2.60 V (vs. Ag/AgCl (5 mol.%), the same below) for Li^+ ion electrodeposition and +1.05 V for Cl^- ion oxidation. In the LiCl-KCl-$LaCl_3$-$MgCl_2$ melt, Mg(II) ions would be expected to first deposit on the tungsten electrode based on relative standard potentials for Mg(II)/Mg and La(III)/La. What were observed in this plot are one steep rising and slow decaying cathodic peak (Peak A) and one corresponding stripping anodic peak (peak A') shown at -2.02 and -1.87 V, respectively. This supports the conclusion that the reduction of Mg(II) ions to Mg metal is a one-step process, and Mg(II) is the only stable electroactive state in the large electrochemical window of the LiCl-KCl melt, as has been observed by other researchers.[9] Mg tends to interact with other metals from the melt to form multiple forms of alloys after electroreduction.[10,11] As the potential goes more negative than -2.09 V, significant interaction between the La^{3+} and Mg^{2+} ions are observed in Figure 1. The additional peak (at -2.15 V) between the typical reduction peaks for La(III)/La (at -2.26 V) and Mg(II)/Mg (at -2.02 V) reactions is thus presumed to be the underpotential deposit (UPD) of La(III) ions on the Mg metal.[8,9,12]

Chronopotentiometry

This conclusion was also supported by the CP-OCP curve recorded on a tungsten rod in the LiCl-KCl-$LaCl_3$ ($5.80x10^{-5}$ mol/cm^3)-$MgCl_2$ ($5.61x10^{-5}$ mol/cm^3) melt at 773 K that is shown in Figure 2. The chronopotentiogram was recorded with a cell current of -80 mA, which resulted in three observed potential plateaus. These correspond to the depositions of Mg(II) ions on the tungsten electrode at -2.02 V, the UPD of La(III) ions on the Mg metal at -2.15 V, and the deposition of La(III) ions on the tungsten electrode at

-2.26 V. Three potential plateaus also appeared in the potential profile when the OCP was recorded afterward, as shown in the inset of Figure 2.

Surface Area Determination

Since concentration correlations are based on current density measured at the working electrode (WE), precision of concentration measurement is limited by precision of the known, measured, or assumed value of the WE area. When using a rod with a known diameter for the WE, the key parameter to measure is the immersion depth. To improve the accuracy in determining the immersion depth of WE, the tungsten electrode was connected to a VXM stepping motor controller. And a cyclic voltammogram with a scan rate of 0.2 V/s was recorded each time the WE was moved up 1 mm by using the controller. The peak height for Mg(II)/Mg reaction was then determined and linearly correlated as a function of the changes in the immersed depth, as shown in Figure 3.

The electrodeposition of Mg(II) ions on the tungsten electrode has been proven to be reversible when the scan rate is less than 0.3 V/s.[9] In this case, the Berzins-Delahay equation (Equation. 1) could be used to quantitatively describe the relationship between the peak current and the scan rate.[13]

$$i_p = -0.6105\left(\frac{nF}{RT}\right)^{\frac{1}{2}} nAFD^{\frac{1}{2}}C^{*}\upsilon^{\frac{1}{2}} = k \cdot A = k \cdot \pi d\left(\frac{d}{4} + h\right) = k' \cdot (\frac{d}{4} + h) \qquad [1]$$

where i_p, A, n, F, R, T, D, C^*, ν, d and h are peak current (A), surface area of WE (cm^2), electron transfer number, Faraday constant (96,485 C/mol), gas universal constant (8.314 J/mol-K), Kelvin temperature (K), diffusion coefficient (cm^2/s) of Mg(II) ion (cm^2/s), bulk concentration of Mg(II) ion (mol/cm^3), scan rate (V/s), diameter and the immersion depth of WE, respectively.

Using the curve fit from Figure 3, the initial immersion depth was determined to be 16.55 mm, and the WE was moved up 6 mm in total by using the VXM controller, thus

the final immersion depth was 10.05 mm, and the surface area was then calculated to be 0.663 cm^2.

Sampled Current Voltammetry

Besides the CV and CP-OCP methods, sampled-current voltammetry (SCV) was carried out in the LiCl-KCl-$LaCl_3$-$MgCl_2$ melt at 773 K. In the SCV, a series of step potentials ranging from -1.90 to -2.40 V with an increase step of -0.10 V were applied to the system, and the perspective current-time response was recorded. Then the dependence of the response current on the applied potential was examined at sampled time of 0.3 s, as shown in Figure 4.

In the sampled-current voltammogram shown in Figure 4, seven regions are observed as the potential decreases from -1.90 to -2.40 V. When E>-1.95 V, no reduction occurs. Only minor charging current shows up, and the sampled current is close to zero. When -1.95 <E< -2.03 V, only Mg(II) ions can be deposited on the WE, but the kinetics are not fast enough to reduce the surface concentration of Mg(II) ions to be zero. When -2.03 <E< -2.06 V, the response current levels off, possibly indicating that the electrodeposition of Mg(II) ions is under mass-transfer control. As potential goes more negative, the UPD of La(III) ions on the Mg metal becomes more significant, and the second plateau is formed from -2.12 to -2.16 V. When the step potential becomes more negative than -2.25 V, another current plateau is formed, corresponding to the electrodeposition of La(III) ions onto La metal.

In the mass-transfer limited regions, the Cottrell Equation (Equation 2) is applicable for the quantitative description of the relationship between the response current and time.[14]

$$\mathrm{j(t)} = i(t)/A = \frac{nFD^{1/2}C^*}{\pi^{1/2}} \cdot t^{-1/2} = k_{CA} \cdot t^{-1/2} \qquad [2]$$

where j(t), i(t), A, n, F, D, C^*, and t are response current density (A/cm^2) at time t, response current (A) at time t, working electrode area (cm^2), electron transfer number, Faraday constant, diffusion coefficient of La(III) ion (cm^2/s), bulk concentration of La(III) ion (mol/cm^3), and time (s), respectively.

In Figure 4, plateaus B and C both involve the diffusion of La(III) ions from the bulk to the surface of WE, thus they should be combined in evaluating the concentration of La(III) ions. The k_{CA}'s based on Equation 2 were correlated from the $j(t) \sim t^{-1/2}$ plots at various potentials determined from the sampled-current voltammogram. The regressed k_{CA} at potential of -2.04 V was treated as k_{CA} for the Mg(II)/Mg reaction, and the difference between the regressed k_{CA}'s at potentials of -2.04 and -2.29 V was treated as k_{CA} for the La(III)/La reduction process. All the determined k_{CA}'s for Mg(II)/Mg and La(III)/La were plotted in Figure 5 as a function of the concentration of $LaCl_3$ or $MgCl_2$. The average diffusion coefficients of La(III) and Mg(II) ions were calculated by substituting the regressed slopes in Figure 5 into the Equation 2. These diffusion coefficients are listed in Table I.

Normal Pulse Voltammetry

Figure 6 presents an overlay plot with a typical normal pulse voltammogram and a cyclic voltammogram recorded on a tungsten electrode in the LiCl-KCl melt with 1.93×10^{-4} mol/cm^3 $LaCl_3$ and 5.12×10^{-5} mol/cm^3 $MgCl_2$. For each NPV test, the step potential was set to be -0.01 V, and the interval time was fixed to be 10 s.

In comparison with the ones recorded with low concentrations of $LaCl_3$ and $MgCl_2$, the normal pulse voltammogram and cyclic voltammogram with higher concentration of analyte become more complicated, and a tiny shoulder was observed on the positive side of the peak or plateau for La(III)/La. This shoulder is believed to be due to formation of another La-Mg alloy. If this is true, plateaus B, C, and D all represent the diffusion of La(III) ions from the bulk to the surface of WE, and the diffusive current for La(III) and

Mg(II) deposition process were determined using the method shown in Figure 6. For each plateau, the diffusive current could be given by the Cottrell Equation as[14]

$$j_d = i_d/A = \frac{nFD^{1/2}C^*}{\pi^{1/2}} \cdot \tau^{-1/2} = k_{NPV} \cdot \tau^{-1/2} \qquad [3]$$

where j_d, i_d, A, n, F, D, C^*, and τ are diffusive current density (A/cm^2), diffusive current (A), working electrode surface area (cm^2), electron transfer number, Faraday constant, diffusion coefficient of La(III) or Mg(II) ion (cm^2/s), bulk concentration of La(III) or Mg(II) ion (mol/cm^3), and pulse time (s), respectively.

The k_{NPV}'s in Equation 3 were correlated and plotted as a function of the concentration of $LaCl_3$ and $MgCl_2$ in Figure 7. Using the regressed slope in Figure 7, the average diffusion coefficients of La(III) and Mg(II) ions were calculated and are listed in Table I.

Concentration Measurement

In our previous work, CA and NPV were proven to be very promising for concentration prediction for molten salt mixture containing multiple components.[8] In this work, they were applied to the LiCl-KCl-$LaCl_3$-$MgCl_2$ system. For this purpose, tests were run in LiCl-KCl melt with 18 sets of different compositions of $LaCl_3$ and $MgCl_2$, as listed in Table II. Tests 1-15 were used for calibration, from which the average diffusion coefficients of La(III) and Mg(II) ions were calculated, as shown in Figures. 5, 7, and Table I. Tests 16-18 were treated as unknowns. Using the calculated diffusion coefficients in Table I, the composition of $LaCl_3$ and $MgCl_2$ in Tests 16-18 were predicted using the Cottrell Equation and were compared to the ICP measured values in Table III.

It can be seen that CA and NPV both exhibit excellent performance in concentration prediction for the LiCl-KCl-$LaCl_3$-$MgCl_2$ mixture with errors less than 4%. It should be noted that the significant interaction between the La(III) and Mg(II) ions does make it

very difficult to determine the peak height via CV and the plateau height via NPV and SCV for La(III)/La. And this problem would be expected to further worsen with increasing concentration of $LaCl_3$ or $MgCl_2$. The minor differences in potentials for Mg(II)/Mg, UPD of La(III) ions on Mg metal and La(III)/La make the plateaus in the chronopotentiogram very close to each other, and the transition time could hardly be determined accurately. Thus, the CV and CP data was not adopted for further calculation. For application of the CA and NPV methods, all the plateaus for the UPD of La(III) ions on Mg metal were treated as contributions to the deposition of La(III) ions, but the rationality of this approach needs to be further considered and verified.

Conclusions

Molten salt mixtures containing $MgCl_2$ and $LaCl_3$ in eutectic LiCl-KCl have been prepared with varying compositions and analyzed electrochemically using cyclic voltammetry, chronopotentiometry, chronoamperometry, sampled current voltammetry, and normal pulse voltammetry. The object has been to develop correlations between voltammetry sensor output and concentration of the solutes in the molten salt. These correlations can form the basis for real time sensors in molten salt electrorefiners, such as those used for processing spent nuclear fuel.

For the La/Mg system, underpotential deposition of La onto Mg results in additional reduction and oxidation peaks for cyclic voltammetry. The current contribution by each reduction transition was best-resolved using normal pulse voltammetry. Using this method, the total limiting current for La(III) reduction was a summation of contributions from two underpotential deposition transitions and the primary reduction reaction. By fitting the Cottrell equation to each limiting current value, a concentration correlation was derived. The fit to the Cottrell equation was excellent for both $LaCl_3$ and $MgCl_2$ concentrations with correlation factors of 0.999. By splitting the data into a calibration set

and a set of unknowns, concentration measurement error was determined to be from 0.25 to 3.69%. This is, thus, an excellent candidate for real time monitoring of salt compositions in molten salt electrorefiners. More complicated salt mixtures will be investigated using the same approaches developed for two solute salts.

Acknowledgements

Funding from the Department of Energy's Nuclear Energy University program is acknowledged for supporting experimental investigations. Also, the financial support provided by China Scholarship Council (CSC) during a visit of Zhonghang Wang (No. 201404910406) to University of Utah (UU) is acknowledged.

References

1. S.X. Li and M.F. Simpson.; "Anodic Process of Electrorefining Spent Nuclear Fuel in Molten LiCl-KCl-UCl_3/Cd System;" *Journal of Mineral and Metallurgical Processing*, **22**, no.4, November 2005 (2005).
2. R.W. Benedict, C. Solbrig, B. Westphal, T.A. Johnson, S.X. Li, K. Marsden, and K.M. Goff, (2007). Pyroprocessing progress at Idaho national Laboratory. *Advanced Nuclear Fuel Cycles and Systems (GLOBAL 2007)* (2007).
3. D. Vaden, R.W. Benedict, K.M. Goff, R.W. Keyes, and R.D. Mariani; "Material Accountancy in an Electrometallurgical Fuel Conditioning Facility;" *Proceedings of DOE Spent Nuclear Fuel and Fissile Material Management*, 376-382 (1996).
4. M. Iizuka, T. Inoue, O. Shirai, T. Iwai, and Y. Arai, "Application of Normal Pulse Voltammetry to On-line Monitoring of Actinide Concentrations in Molten Salt Electrolyte," *J. Nucl. Mater.,* **297**, pp. 43-51 (2001).
5. M.M. Tylka, J.L. Willit, J. Prakash, and M.A. Williamson; "Application of Voltammetry for Quantitative Analysis of Actinides in Molten Salts;" *J. Electrochemical Society*, **162** (12) H852-H859 (2015).

6. D.H. Kim, S.E. Bae, T.H. Park, J.Y. Kim, C.W. Lee, and K. Song; “Real-time monitoring of metal ion concentration in LiCl-KCl melt using electrochemical techniques;” *Microchemical Journal*, **114**, May 2014, 261-265 (2014).
7. D. Rappleye, S.-M. Jeong, M. Gonzalez, L.C. Hansen, and M.F. Simpson; "Application of Voltammetry to Measurement of Concentrations of Multiple Lanthanide Ions in Molten LiCl-KCl," *J. Nucl. Fuel Cycle Waste Technol.,* **13**, no. S, pp. 29-38 (2015).
8. Z. Wang, D. Rappleye, and M.F. Simpson; "Voltammetric Analysis of Mixtures of Molten Eutectic LiCl-KCl Containing $LaCl_3$ and $ThCl_4$ for Concentration and Diffusion Coefficient Measurement," *Electrochim. Acta,* **191**, pp. 29-43 (2016).
9. H. TANG, Y.D. Yan, M.L. Zhang, Y. Xue, Z.J. Zhang, W.C. Du, and H. He, Electrochemistry of $MgCl_2$ in LiCl-KCl Eutectic Melts. *Acta Phys. -Chim. Sin*., **29**(08): p. 1698-1704 (2014).
10. A.M. Martínez, B. Borresen, G.M. Haarberg, Y. Castrillejo, and R. Tunold, Electrodeposition of magnesium from the eutectic LiCl–KCl melt. *Journal of Applied Electrochemistry*. **34**(12): p. 1271-1278 (2004).
11. Y. De Yan, M.L. Zhang, Y. Xue, W. Han, D.X. Cao, and S.Q. Wei, Study on the preparation of Mg–Li–Zn alloys by electrochemical codeposition from LiCl–KCl–$MgCl_2$–$ZnCl_2$ melts. *Electrochimica Acta*, 2009. **54**(12): p. 3387-3393.
12. H. Tang and B. Pesic, Electrochemical behavior of $LaCl_3$ and morphology of La deposit on molybdenum substrate in molten LiCl–KCl eutectic salt. *Electrochimica Acta*, 2014. **119**(0): p. 120-130 (2009).
13. P. Delahay, *New instrumental methods in electrochemistry: theory, instrumentation, and applications to analytical and physical chemistry*, Interscience Publishers (1954).
14. A.J. Bard and L.R. Faulkner, *Electrochemical Methods: Fundamentals and Applications*, Wiley (2000).

Table Captions

Table I. Average diffusion coefficient of La(III) and Mg(II) ions in LiCl-KCl-$LaCl_3$-$MgCl_2$ melt at 773K calculated from CA and NPV data

Table II. Mixture composition for the La/Mg tests

Table III. Mixture composition prediction using the calculated average diffusion coefficients from CA and NPV

Table I.

Ions	Conc., 10^{-4} mol/cm^3	Diffusion coefficient, 10^{-5} cm^2/s	
		CA	NPV
La(III)	0.58-3.14	1.31±0.03	2.01±0.04
Mg(II)	0.46-1.94	2.46±0.07	3.89±0.06

Table II.

Test No.	Conc., 10^{-4} mol/cm^3		Test No.	Conc., 10^{-4} mol/cm^3	
	$LaCl_3$	$MgCl_2$		$LaCl_3$	$MgCl_2$
1	0.580	0.561	10	1.769	1.126
2	1.308	0.545	11	2.690	1.471
3	1.927	0.512	12	3.075	1.492
4	2.370	0.496	13	0.706	1.121
5	3.093	0.463	14	0.940	
6	3.108	1.080	15	0.640	1.972
7	3.135	1.938	16	1.422	1.772
8	0.600	0.985	17	1.895	1.844
9	1.223	0.868	18	2.411	1.745

Table III.

Test No.	Measured Conc., 10^{-4} mol/cm^3		Predicted Conc., 10^{-4} mol/cm^3		Relative error, %		Remark
	$LaCl_3$	$MgCl_2$	$LaCl_3$	$MgCl_2$	$LaCl_3$	$MgCl_2$	
16	1.42	1.77	1.40	1.75	-1.56	-1.28	
17	1.90	1.84	1.94	1.81	2.19	-1.63	CA
18	2.41	1.75	2.48	1.74	2.99	-0.25	
16	1.42	1.77	1.37	1.72	-3.69	-2.71	
17	1.90	1.84	1.94	1.83	2.41	-0.63	NPV
18	2.41	1.75	2.47	1.78	2.55	1.87	

Figure Captions

Figure 1. Comparison of cyclic voltammograms recorded in pure LiCl-KCl and LiCl-KCl-$LaCl_3$-$MgCl_2$ melts at 773 K ($LaCl_3$ concentration: $5.80x10^{-5}$ mol/cm^3, $MgCl_2$ concentration: $5.61x10^{-5}$ mol/cm^3, scan rate: 0.2 V/s)

Figure 2. Chronopotentiogram on W electrode in LiCl-KCl-$LaCl_3$-$MgCl_2$ melt at 773K, driving current -80 mA. Inset: OCP on W electrode in LiCl-KCl-$LaCl_3$-$MgCl_2$ melt at 773K. (WE area: 0.663 cm^2, $LaCl_3$ concentration: $5.80x10^{-5}$ mol/cm^3, $MgCl_2$ concentration: $5.61x10^{-5}$ mol/cm^3)

Figure 3. Correlation of the peak heights and the changes in immersed depth of WE ($LaCl_3$ concentration: $5.80x10^{-5}$ mol/cm^3, $MgCl_2$ concentration: $5.61x10^{-5}$ mol/cm^3, scan rate: 0.2 V/s)

Figure 4. Sampled-current voltammogram on tungsten electrode in LiCl-KCl-$LaCl_3$-$MgCl_2$ melt at 773 K ($LaCl_3$ concentration: $5.80x10^{-5}$ mol/cm^3, $MgCl_2$ concentration: $5.61x10^{-5}$ mol/cm^3, WE area: 0.663 cm^2)

Figure 5. Correlated k_{CA} in Eq. 2 for LiCl-KCl-$LaCl_3$-$MgCl_2$ melt at 773 K as a function of concentration of $LaCl_3$ and $MgCl_2$

Figure 6. Normal pulse voltammogram and cyclic voltammogram recorded on tungsten electrode in LiCl-KCl-$LaCl_3$-$MgCl_2$ melt at 773 K ($LaCl_3$ concentration: $1.93x10^{-4}$ mol/cm^3, $MgCl_2$ concentration: $5.12x10^{-5}$ mol/cm^3, WE area: 0.657 cm^2, pulse time: 0.30 s, step potential: 0.01 V, interval time: 10 s)

Figure 7. Correlated k_{NPV} in Eq. 3 for LiCl-KCl-$LaCl_3$-$MgCl_2$ melt at 773 K as a function of concentration of $LaCl_3$ and $MgCl_2$

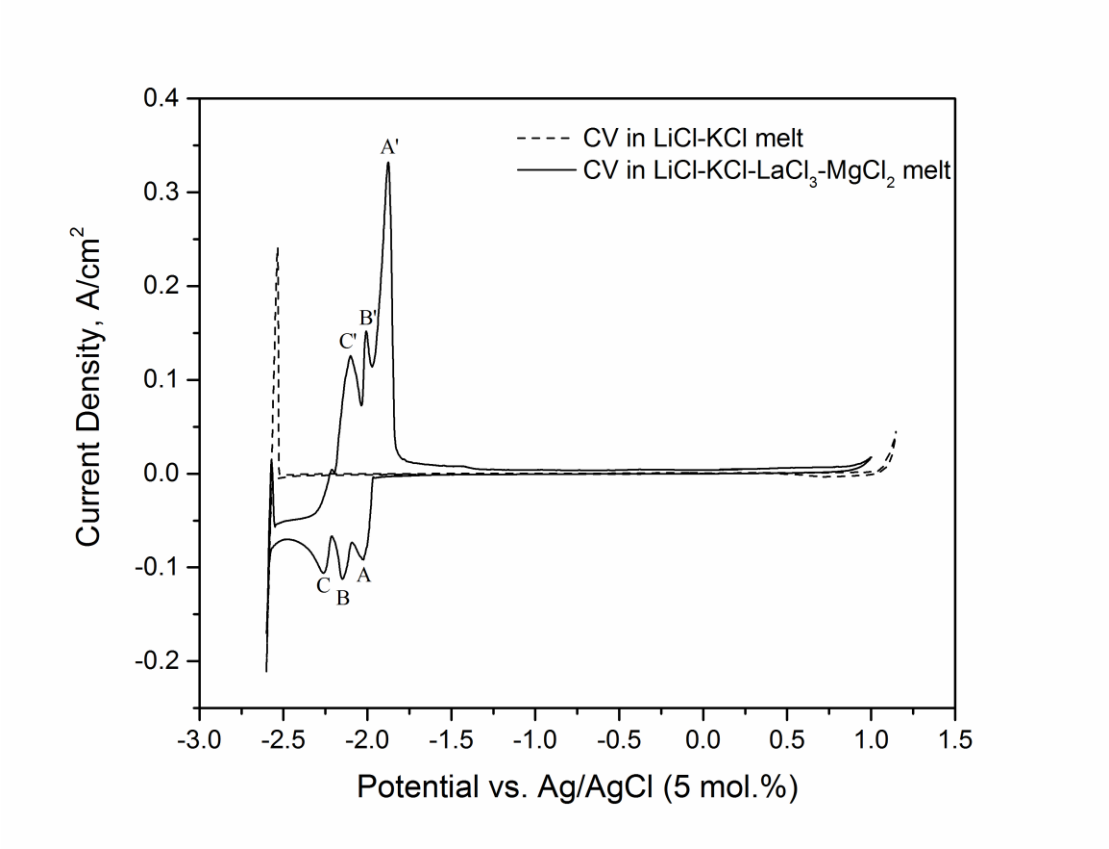
CV in LiCl-KCl melt
CV in LiCl-KCl-LaCl3-MgCl2 melt
A'
B'
C'
A
B
C
Current Density, A/cm2
Potential vs. Ag/AgCl (5 mol.%)
0.4
0.3
0.2
0.1
0.0
-0.1
-0.2
-3.0
-2.5
-2.0
-1.5
-1.0
-0.5
0.0
0.5
1.0
1.5

Figure 1

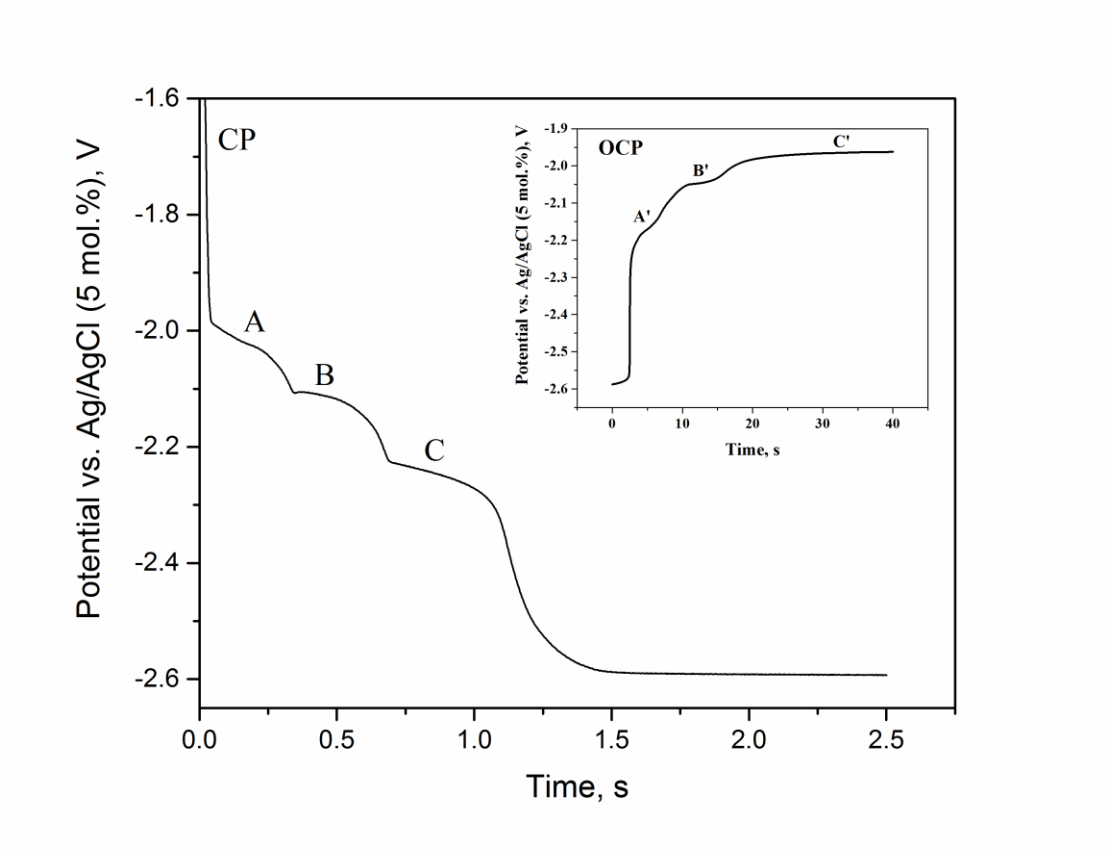

Figure 2

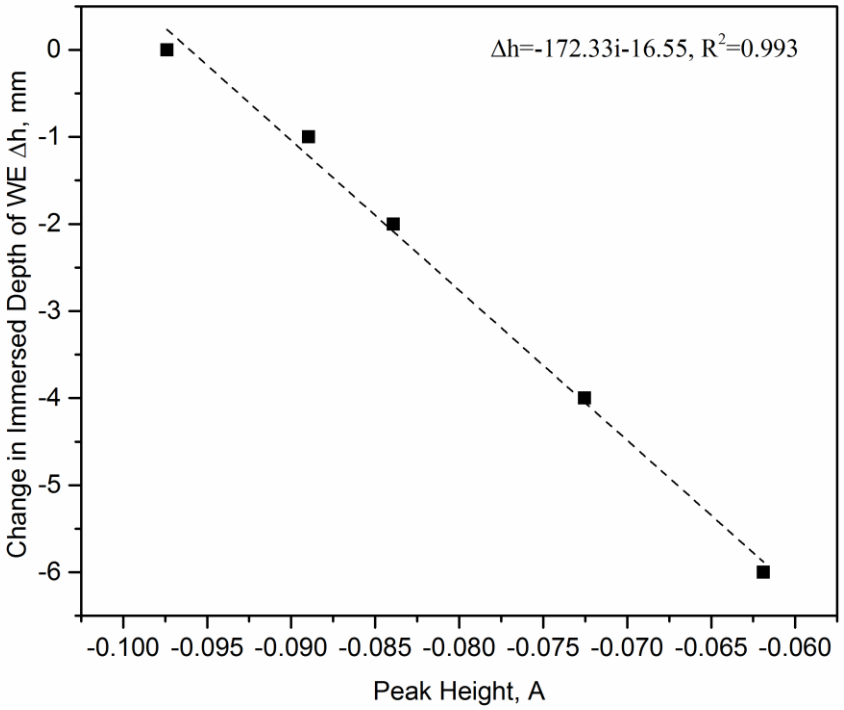
Δh=-172.33i-16.55, R²=0.993
Change in Immersed Depth of WE Δh, mm
0
-1
-2
-3
-4
-5
-6
-0.100 -0.095 -0.090 -0.085 -0.080 -0.075 -0.070 -0.065 -0.060
Peak Height, A

Figure 3

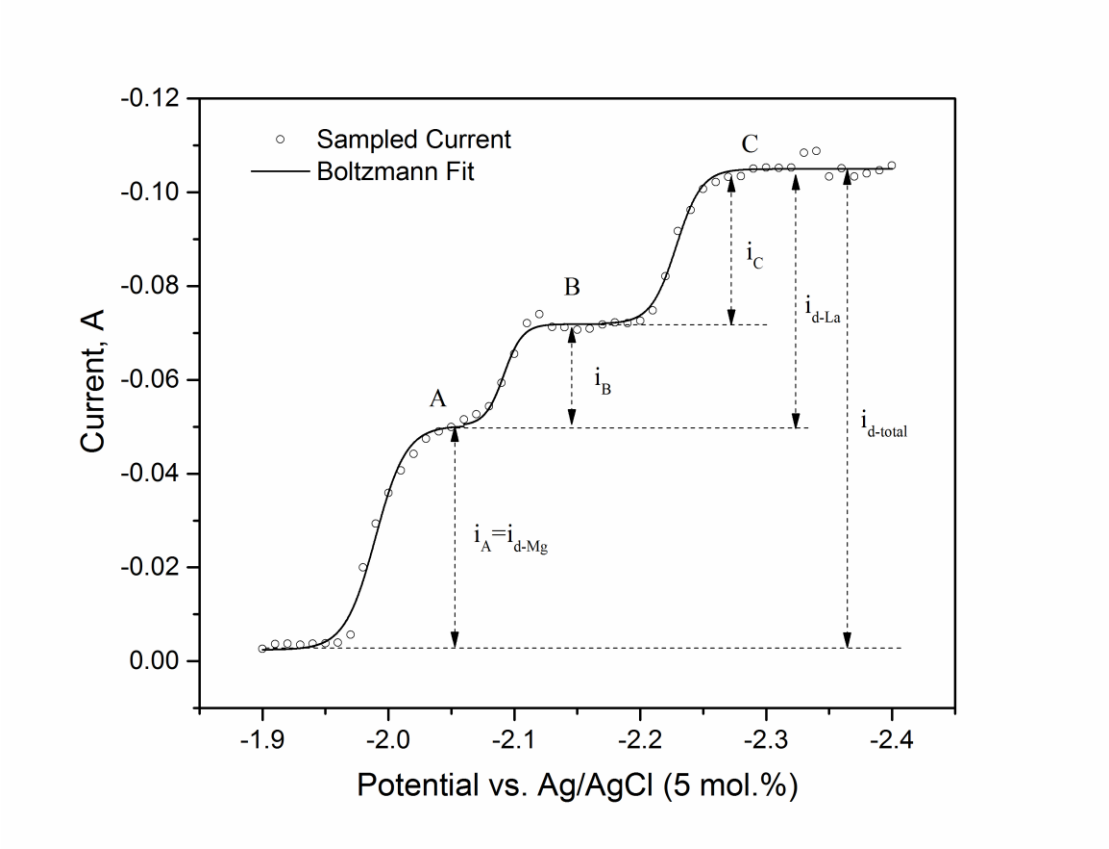
Sampled Current
Boltzmann Fit
A
B
C
$i_A=i_{d\text{-}Mg}$
i_B
i_C
$i_{d\text{-}La}$
$i_{d\text{-}total}$
Current, A
Potential vs. Ag/AgCl (5 mol.%)
-0.12
-0.10
-0.08
-0.06
-0.04
-0.02
0.00
-1.9
-2.0
-2.1
-2.2
-2.3
-2.4

Figure 4

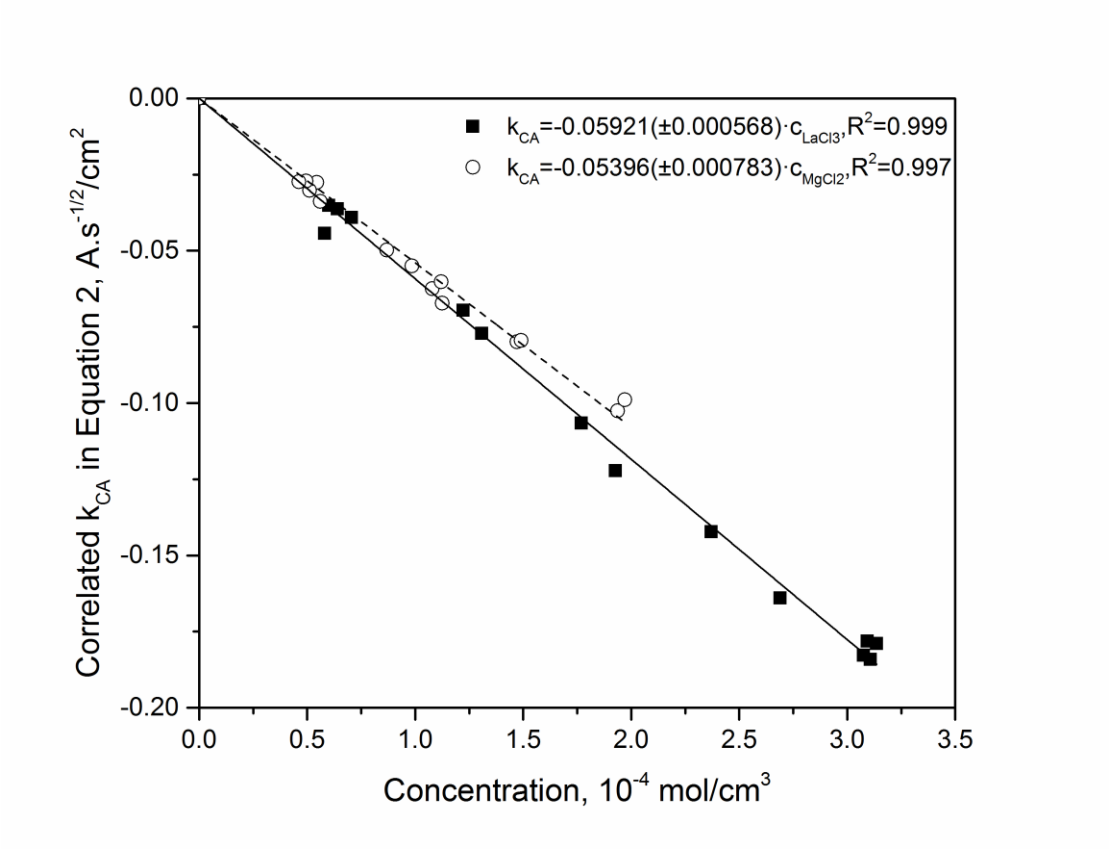
0.00
-0.05
-0.10
-0.15
-0.20
0.0
0.5
1.0
1.5
2.0
2.5
3.0
3.5
Correlated k_{CA} in Equation 2, $A.s^{-1/2}/cm^2$
Concentration, 10^{-4} mol/cm^3
k_{CA}=-0.05921(±0.000568)·c_{LaCl3},R^2=0.999
k_{CA}=-0.05396(±0.000783)·c_{MgCl2},R^2=0.997

Figure 5

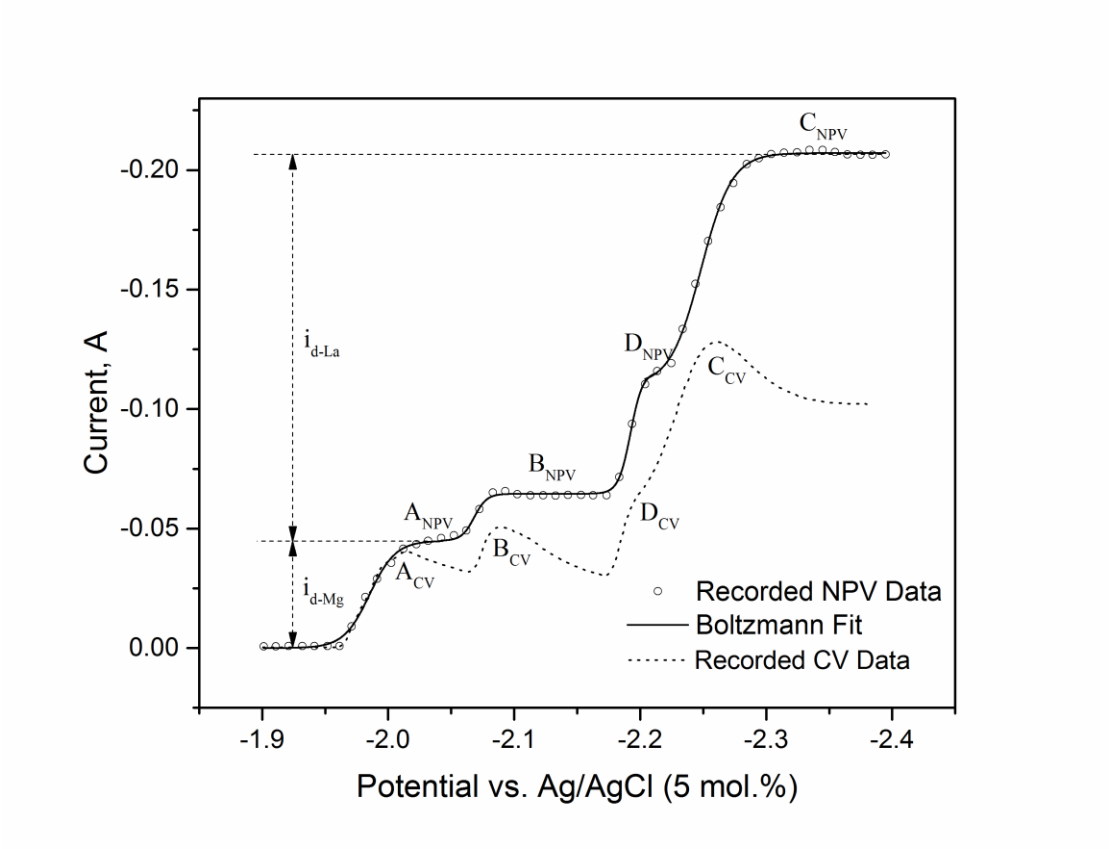
C_NPV
-0.20
-0.15
-0.10
-0.05
0.00
Current, A
i_d-La
D_NPV
C_CV
B_NPV
A_NPV
D_CV
B_CV
A_CV
i_d-Mg
Recorded NPV Data
Boltzmann Fit
Recorded CV Data
-1.9
-2.0
-2.1
-2.2
-2.3
-2.4
Potential vs. Ag/AgCl (5 mol.%)

Figure 6

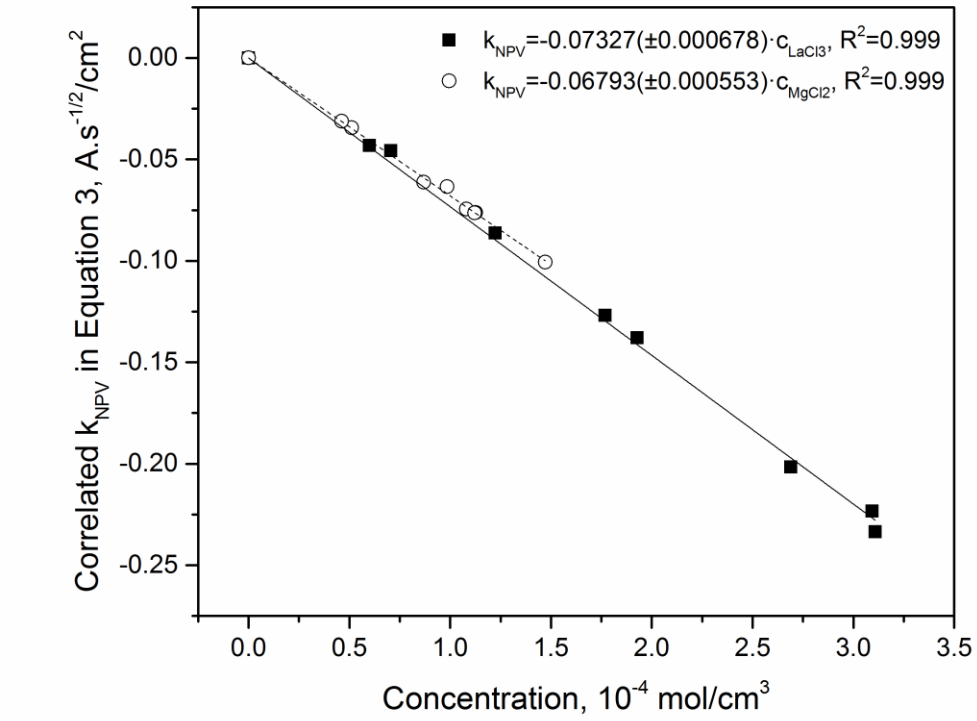
k_{NPV}=-0.07327(±0.000678)·c_{LaCl3}, R^2=0.999
k_{NPV}=-0.06793(±0.000553)·c_{MgCl2}, R^2=0.999
Correlated k_{NPV} in Equation 3, $A.s^{-1/2}/cm^2$
0.00
-0.05
-0.10
-0.15
-0.20
-0.25
0.0
0.5
1.0
1.5
2.0
2.5
3.0
3.5
Concentration, 10^{-4} mol/cm^3

Figure 7